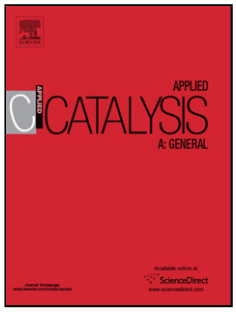

Title: Morphological Control of Inverted MgO-SiO_2 Composite Catalysts for Efficient Conversion of Ethanol to 1,3-Butadiene

Authors: Shenxiao Li, Yong Men, Jinguo Wang, Shuang Liu, Xuefei Wang, Fei Ji, Shanshan Chai, Qiaoling Song

PII: S0926-860X(19)30115-2
DOI: https://doi.org/10.1016/j.apcata.2019.03.007
Reference: APCATA 17012

To appear in: *Applied Catalysis A: General*

Received date: 2 January 2019
Revised date: 12 March 2019
Accepted date: 13 March 2019

Please cite this article as: Li S, Men Y, Wang J, Liu S, Wang X, Ji F, Chai S, Song Q, Morphological Control of Inverted MgO-SiO_2 Composite Catalysts for Efficient Conversion of Ethanol to 1,3-Butadiene, *Applied Catalysis A, General* (2019), https://doi.org/10.1016/j.apcata.2019.03.007

Morphological Control of Inverted MgO-SiO_2 Composite Catalysts for Efficient Conversion of Ethanol to 1,3-Butadiene

Shenxiao Li, Yong Men*, Jinguo Wang, Shuang Liu, Xuefei Wang, Fei Ji, Shanshan Chai, Qiaoling Song

College of Chemistry and Chemical Engineering, Shanghai University of Engineering Science, Shanghai 201620, P. R. China

*Authors to whom correspondence should be addressed. E-mail addresses: men@sues.edu.cn, Fax: +86-21 6779 1215; Tel: +86-21 6787 4046

Graphical abstract

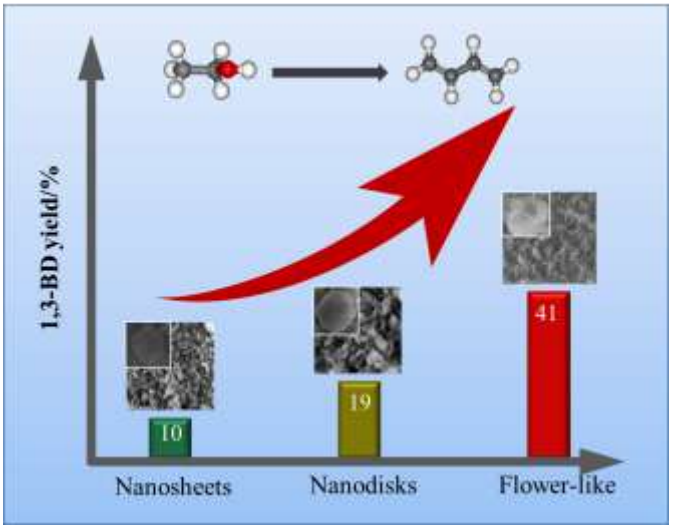

The effect of MgO precursor morphologies was explored for conversion of ethanol to 1,3-BD. Extensive characterizations demonstrate that the unique layered flower-like architectures may facilitate the formation of interfacial Mg-O-Si species and enhance Lewis basicity on the bridged O in Mg-O-Si bond via the strong interaction between MgO and SiO_2 in binary MgO-SiO_2 composite catalysts which are favorable for the superior activity.

Highlights:

- Synthesis of three novel MgO-SiO_2 composite catalysts by reverse incipient wetness impregnation.
- MgO-SiO_2 composite catalysts exhibited remarkable morphology-dependent reactivity for Lebedev reaction.
- The MgO precursors with different morphologies affect the physicochemical properties of the catalyst surface.
- The unique layered structure of the flower-like catalyst is more favorable for 1, 3-butadiene formation.
- The Mg-O-Si bond formed plays a crucial role in the formation of 1,

3-butadiene.

Abstract:

In this work, three novel MgO-SiO_2 composite catalysts with inverted structure have been synthesized via a facile and scalable strategy by means of the incipient wetness impregnation of the silica sol onto MgO precursors with different morphologies, and evaluated for the one-step conversion of ethanol to 1,3-butadiene. The prepared flower-like MgO-SiO_2 composite catalysts exhibited highly enhanced catalytic activity than those catalysts synthesized from MgO precursors with nanodisks and nanosheets morphologies. Characterization results based on XRD, FT-IR, UV–vis, BET, CO_2-TPD, NH_3-TPD, ethanol-TPD, and ^{29}Si MAS NMR revealed that unique layered flower-like architectures may facilitate the formation of interfacial Mg-O-Si chemical bond in binary MgO-SiO_2 composite catalysts which are mainly responsible for the superior activity. This study presents a new strategy to design and develop the catalyst for efficient conversion of bio-ethanol to 1,3-butadiene by morphological control of MgO-SiO_2 bifunctional catalysts.

Keywords: ethanol, 1,3-butadiene, MgO-SiO_2, Mg-O-Si bonds, flower-like, morphological control

1. Introduction

1,3-Butadiene (BD) is an important monomer in the synthesis of polymer industry. Self-polymerization of butadiene and polymerization with other olefin monomers has shown great commercial value.[1] BD mainly used for the synthesis of styrene-butadiene rubber, polybutadiene and acrylonitrile-butadiene-styrene（ABS） rubber, and also applied in the Diels-Alder reaction to form cycloalkanes and cycloalkanes.[2-5] At present, BD is mainly derived from the naphtha steam cracking produces byproducts of the ethylene process. Isolation of butadiene from the other products requires a number of expensive extractive distillation steps.[6] However, the predicted shift towards lighter feeds for steam cracking and the increased usage of shale gas as an alternative source for ethylene have resulted in a supply shortage and consequent price increase for BD.[7] In order to meet the market demand of BD, looking for an alternative solution to produce BD, a renewable and nonpetroleum rooted route is highly desirable. The Lebedev reaction path using bioethanol to convert to BD in one step (Scheme 1) has been extensively studied in the early twentieth century by using mixed metal oxides as catalysts, typically MgO/SiO_2, because bio-ethanol can be obtained via fermentation of carbohydrates (sugar and corn etc.) or the cellulosic.[8-10]

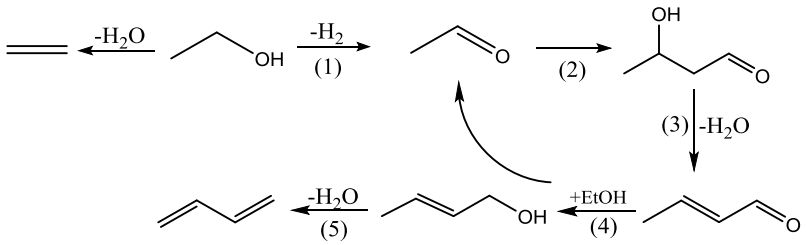

Scheme 1. Generally accepted reaction network for the Lebedev process.

At present, various types of catalysts have been reported to perform the reaction, including $Ag/ZrO_2/SiO_2$,[11] ZrBEA zeolite,[12] $ZnZr/MgO\text{-}SiO_2$,[13] and $Hf\text{-}Zn/SiO_2$[14] catalysts. Magnesia-silica catalysts were intensively investigated by many research groups,[2, 4] and typically performed well in terms of butadiene production yield, demonstrated to be very efficient for the direct conversion of ethanol to BD, whose performance was also affected greatly by the preparation method. The preparation method and compositions of $MgO\text{-}SiO_2$-based systems are considered to be crucial factors for their performance.[15] Among many methods for synthesizing catalysts, including wet-kneading method,[1, 16-20] sol-gel method,[15, 21]co-precipitation method,[19, 22-23] incipient wetness impregnation method[1] and physical mixing method,[1, 17] etc., the wet-kneading has been demonstrated to be a very efficient method for producing $MgO\text{-}SiO_2$ catalysts for the process of ethanol-to-butadiene since the first discovery by Natta et al. [19, 24-26]. In recent years, the sol-gel method has been reported as one of the effective preparation methods. Ochoa and co-workers[15] investigated that the activity of different ratios of $MgO\text{-}SiO_2$ catalyst prepared by sol-gel method and explained in terms of acid/basic catalyst requirements. However, the preparation of $MgO\text{-}SiO_2$ by incipient wetness impregnation is usually studied as a comparative

method, and it is rarely discussed as a major preparation method because the selectivity of BD obtained by this method is generally low.

In a heterogeneously catalyzed multistep cascade reaction system, the catalytic activity and selectivity are often enhanced by synergistic effects through which different active phases or sites can function in a concerted manner to encompass all the necessary catalytic functionalities.[27-28] Bifunctional catalysts operate by utilizing two different types of catalytic sites on the same solid. Extensive research revealed that the basic function of MgO-SiO_2 catalyzes dehydrogenation/condensation/MPV reduction of ethanol and intermediates, whereas the acidic function of the composite facilitates dehydration of 3-hydroxybutanal to crotonaldehyde and crotyl alcohol.[16, 19, 29] Obviously, for such a complex reaction network step, the synergy of the catalyst plays a crucial role in the reaction. It has been reported in the literatures that the difference in the preparation methods and compositions of the catalysts leads to a delicate balance of different active sites (acidic, basic, and redox) on the catalyst surface that is indispensable for the Lebedev reaction process.[30] Although a large number of studies have been conducted on the MgO-SiO_2 system, the detailed structure-activity relationship has not yet been fully elucidated and needs further study.

Studies have shown that the difference in catalyst structure due to the difference in morphology has a great influence on the activity of the catalyst. In recent years, the controlled synthesis of nano- or micro sized metals and metal oxides with different morphologies has received great research interests in the use of catalysis.[31-32] Recently,

there has been extensive research into morphology control of nano-catalyst in tuning the catalytic properties of a nanocatalyst in structure-sensitive reactions.[33] Therefore, developing facile and template-free methods for morphology- and structure-controlled synthesis is of particular interest.

In general, the MgO-SiO_2 composite catalysts can be prepared via the conventional incipient wetness impregnation method by impregnating magnesium salt precursor solutions onto the relatively inert component SiO_2. Herein, to provide further insight on the design principle of MgO-SiO_2 catalysts, three catalysts with inverted structure and different morphologies of flower-like, nanodisks and nanosheets MgO precursors were prepared by facile incipient wetness impregnation of silica sol onto the respective carrier and evaluated for the direct conversion of ethanol to BD. A unique layered structure can be formed by the method of incipient wetness impregnation with the appropriate MgO precursor with the flower-like morphology. As demonstrated by various physicochemical characterizations, the morphology of MgO-SiO_2 catalysts was identified to play a crucial role in the extent of synergy of MgO and SiO_2 which favors the formation of large amounts of Mg-O-Si interfacial bonds and dictates the catalytic performance of the catalyst.

2. Experimental Section

2.1. Materials

Ethylene glycol (EG), $Mg(CH_3COO)_2{\bullet}4H_2O$, ethanol, polyvinylpyrrolidone (PVP, K30) $MgCl_2{\cdot}6H_2O$, ethylenediaminetetraacetic acid disodium salt, benzoic acid,

ammonium hydroxide and NaOH were purchased from Aladdin Chemistry Co. Ltd. (Shanghai, China),Silica Sol was purchased from Jiyida Silicone Reagent Factory (Qingdao, China). All of the chemicals used as received without further purification.

2.2. Catalyst Preparation

The MgO precursors were synthesized by a hydrothermal process with the aid of surfactants.[34-35] Typically, for flower-like MgO precursor, 3.424 g magnesium acetate ($Mg(CH_3COO)_2•4H_2O$) dissolved in 80 mL ethylene glycol, while adding 2.656 g PVP, stirring at room temperature for 30 min, then ultrasonic for 30 min, and finally the resulting clear transparent solution was transferred into a 100 mL Teflon-lined stainless-steel autoclave, the oven was maintained at 180 °C for 4 h, after natural cooling to room temperature, the solid was collected, washed and centrifuged with anhydrous ethanol for several times, and then dried in an oven at 100 °C for 12 h to obtain magnesium oxide precursor. In the case of nanodisks MgO precursor, the ethylenediaminetetraacetic acid disodium salt was used as the surfactant. 2 g of $MgCl_2·6H_2O$ and 0.1 g of surfactant were dissolved in 70 mL of deionized water, stirred at room temperature for 20 min, and then 10 mL of aqueous ammonia was added dropwise to form a white precipitate. For the synthesis of nanosheets MgO precursor, 2 g of $MgCl_2·6H_2O$ and 0.12 g of benzoic acid were dissolved in 60 mL of deionized water, stirred at room temperature for 10 min, and then 20 mL (2 M) of sodium hydroxide solution was added dropwise to form a white precipitate. For each sample, the suspension was transferred to a 100 mL stainless steel autoclave and held

at 180 °C for 24 h. After cooling to room temperature, filter, wash with water, dry at 80 °C for 12 h, MgO precursor were obtained.

The catalyst with molar ratio (Mg/Si) of 1.34 was made by incipient wetness impregnation method. During the preparation of the catalyst, we impregnated the silica sol as a solution onto the magnesium oxide precursor, then allowed to stand at room temperature for 12 h, dried at 80 °C for 12 h, and finally calcined at 500 °C for 4 h in an air atmosphere.

2.3. Catalyst characterization

X-ray diffraction (XRD) patterns were using a diffraction meter (D/Max-rB) with Cu-Kα radiation (λ=1.54056 Å) at room temperature. The scanning rate was 4°/min and the 2θ was from 10° to 80°.

The specific surface area of the material was determined by applying Brunauer-Emmett-Teller (BET) model on a Micromeritics ASAP 2460 apparatus, and the samples were pretreated for 6 h in nitrogen at 200 °C before analysis. The morphology of the material was determined by field emission scanning electron microscope (FESEM).

The Fourier transform infrared spectroscopy (FT-IR) signal of the MgO-SiO_2 catalyst was recorded on a Nicolet 380 infrared spectrometer (USA). FT-IR spectral signals in the wave number range of 4000-400 cm^{-1} were recorded by diluting the sample in KBr and pressing the sample into the IR chamber.

The spectrum of UV-Visible diffuse reflectance spectroscopy (UV-Vis) was measured on a UV-2450 spectrophotometer (Shimadzu, Japan) with $BaSO_4$ as the background, and the absorption intensity between 200-800 nm was tested.

The acidity and basicity of the catalyst were determined by CO_2-temperature-programmed desorption (CO_2-TPD) and NH_3-temperature-programmed desorption (NH_3-TPD) on a Micromeritics Autochem II 2920 apparatus. The test procedure was performed using a 0.05 g catalyst through a U-shaped fixed-bed quartz micro reactor. First pre-treatment under argon at 500 °C for 1 h, then cooled to 100 °C, pre-adsorption for 1 h at 10% CO_2 (NH_3) /He, switching to He gas, and finally raising the temperature to 900 °C (10 °C /min) to induce desorption of CO_2(NH_3).

To further investigated the reaction course of 1,3-butadiene production, the temperature-programmed desorption of ethanol (ethanol-TPD) was tested. 0.05 g of the catalyst was placed on a U-shaped quartz reactor and pretreated in a 3% O_2/He (20 ml/min) atmosphere at 500 °C for 1 h. Then cooled to 50 °C, Inert gas He (20 ml/min) is purged for 30 min to remove water, impurities, etc. adsorbed on the surface of the material. Then bubbling the ethanol into the U-shaped quartz tube for pulse adsorption, when the ethanol adsorption saturation, in a He (30 ml/min) gas atmosphere, raise the temperature to 900 °C at 10 °C/min, at the same time during the heating process, the exhaust gas was connected to the HPR20 online mass spectrometer to monitor the product in real time. In the on-line mass spectrometer, different mass-to-charge ratios (m/e) were set to be collected to further distinguish

each product by the law of mass cracking, The ratio of mass to charge was set to: hydrogen=2, water=18, helium=4, ethanol=46, acetaldehyde=44, butadiene=54 , crotonaldehyde=70, crotyl alcohol=57, aldol=42, ethylene=28.

Magic-angle spinning nuclear magnetic resonance (MAS NMR) spectra were recorded on a Bruker spectrometer. At this field, the resonance frequency of ^{29}Si is 59.6 MHz; the recycle time is 30 s, and the pulse length is 5.0 μs. The spinning frequency of the rotor is 5 kHz. The catalysts were packed in 4 mm Zirconia rotors. Tetramethylsilane was used as chemical shift reference. The field of ^{29}Si CP MAS NMR spectrum, the resonance frequency of ^{29}Si is 79.5 MHz. 17,000 scans were accumulated with a recycle delay of 10 s. The CP contact time was 4.0 ms, the spinning frequency of the rotor was 10 kHz. For both measurements the samples were packed in 4 mm Zirconia rotors.

A Bruker Tensor 27 FTIR spectrometer was used to collect FTIR-pyridine spectra. About 20 mg of the catalyst sample was pretreated at 450 °C for 1 h. After being cooled down to 50 °C at 50 STP mL min^{-1} He, a background spectra was recorded. Pyridine adsorption took place at 50 °C through a bubbler for 5–10 min while He flowed at 10 STP mL min^{-1}. A pyridine purge took place at 50 °C under a He flow of 50 STP mL min^{-1} for 30 min. Spectra were taken during adsorption to ensure pyridine saturation. Spectra were recorded at 50 °C after 30 min of He purging to remove physisorbed pyridine. The sample temperature was ramped at 10 °C/min to 200 °C and ramped down to 50 °C for spectra collection.

2.4. Catalyst Testing

The conversion of ethanol to 1,3-butadiene (BD) was performed at atmospheric pressure, the reaction reactor was a fixed bed quartz reaction tube having an inner diameter of about 5 mm. Typically, 0.1 g (40-60 mesh particles) of catalyst was placed in the middle of the fixed bed. Nitrogen (50 ml/min) as carrier gas, carrying ethanol (temperature maintained at 20 °C) was passed over the catalyst to on-line gas chromatography(Shimadzu 2014 Gas Chromatography (GC)), and the product was analyzed by one TCD and two FID detectors. The reaction temperature is 300-500 °C, one interval for every 50 °C. Prior to the reaction, the catalyst was pretreated for 30 min at 300 °C.

Kinetic test：The kinetic study was performed in the reaction temperature range of 340-370 °C with the temperatature interval of 10 °C, in order to ensure that the conversion rate of ethanol is less than 12%. The other test conditions were the same as the conditions used for catalytic.

In this paper, the conversion of ethanol and the selectivity of the product are calculated by the following formula, and the carbon balance of the reaction is greater than 95%:

$$Conversion = \frac{\mathrm{Ethanol}_{in} - \mathrm{Ethanol}_{out}}{\mathrm{Ethanol}_{in}} \times 100\% \qquad (1)$$

$$Selectivity = \frac{x_i n_i}{\sum_z x_z n_z} \times 100\% \qquad (2)$$

$$Yield = \mathrm{Conversion} \times \mathrm{Selectivity} \times 100\% \qquad (3)$$

x_i is the mole fraction of products (i); n_z is the number of carbon atoms in carbon-containing products (z).

3. Results and Discussion

3.1. Catalyst characterization

The XRD patterns of all the catalysts samples were demonstrated in Fig. S1. The diffraction pattern of the MgO in the composites exclusively reveals the cubic structure of the percales phase (PDF#45-0946),[1] while the broad peak between 15°-30° is attributed to amorphous phase of SiO_2. It can be seen that both MgO and SiO_2 maintain their individual crystal phase, and in addition to the diffraction peaks of MgO and SiO_2, we also observed diffraction peaks of the proto-enstatite phase on the nanodisks and nanosheets.

The specific surface area, pore volume and pore size distribution of MgO-SiO_2 composites were determined by N_2 adsorption-desorption (Fig. S2) isotherms and summarized in Table 1. The flower-like sample obviously shows the smallest specific surface area, the largest pore volume and pore size than the other two catalysts.Type IV N_2 adsorption-desorption isotherms with H3 hysteresis loop were obtained in all three cases, revealing the presence of mesoporous structure.[30] The large pore size and large pore volume of the flower-like catalyst contribute to the entry of reactant molecules and combine with the active sites on the catalyst surface to promote the occurrence of catalytic reactions.

Table 1 Textural properties of MgO-SiO_2 mixed oxides determined by N_2 adsorption.

Samples	S_{BET} (m^2/g)	V_p (cm^3/g)	D_p (nm)
Flower-like	151	0.59	12.7
Nanodisks	155	0.37	7.60
Nanosheets	161	0.38	7.80

Fig. 1 was a morphological analysis of the catalysts.It can be clearly seen that the flower-like MgO precursor is in the form by ultrathin sheets self-assembly while the nanodisk and nanosheet displayed hexagonal and circular top view with a certain thickness in Fig. 1b and Fig. 1c. Compared with the MgO precursor, the surface of the composite catalyst after loading the SiO_2 became rougher after annealing process. The SEM images of the as-prepared MgO-SiO_2 in Fig. 1d, e, and f show that the final products successfully inherited the architectures of the MgO precursors, presenting the flower-like, nanodisk and nanosheet morphology in Fig. 1a, b and c respectively.

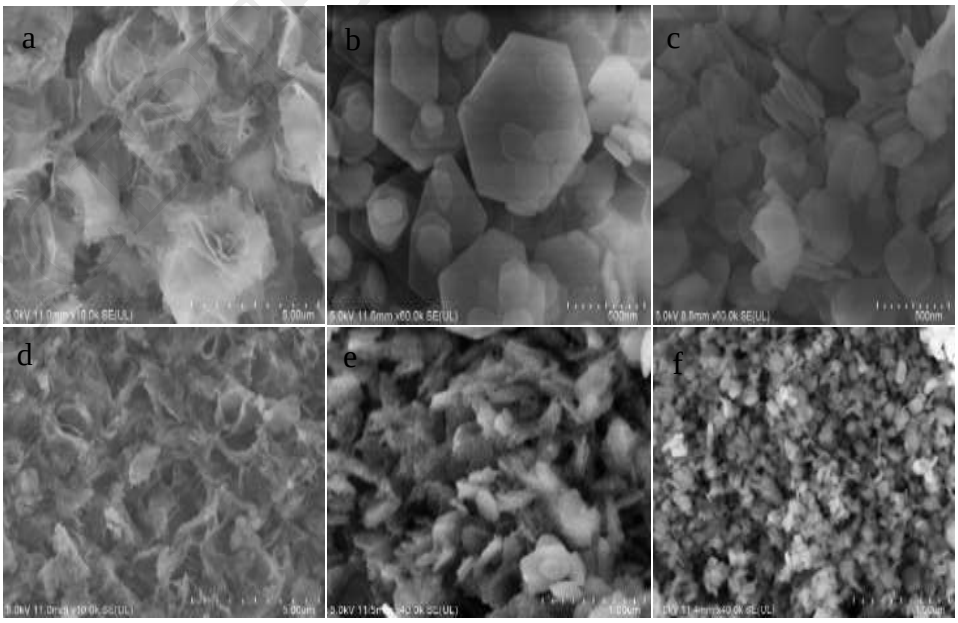

Fig.1. FESEM images of the MgO precursors with three different morphologies (a. Flower-like b. Nanodisks c. Nanosheets) and corresponding MgO-SiO_2 composite catalyst (d. Flower-like e. Nanodisks f. Nanosheets).

The FT-IR spectra of three MgO-SiO_2 composites were collected to provide information on the structural features of the samples between 4000-400 cm^{-1} as shown in Fig. S3. The band at 3400 cm^{-1} can be assigned to the hydroxyl stretching vibration of the water molecules on the catalyst surface,[36-37] and the absorption at 3700 cm^{-1} was attributed to vibration of $Mg(OH)_2$ formed bythe interaction of MgO and water vapor in the air.[38] The peak at 3745 cm^{-1} can be attributed to the silanol group formed by the weak interaction of SiO_2 with water adsorbed on its surface.[37, 39] The peak at 680 cm^{-1} was the stretching vibration of the Mg-O bond.[40] The absorption peaks around 1100 cm^{-1} and 796 cm^{-1} can be assigned to the symmetrical stretching vibration of Si-O-Si bonds whose signal is dependent on the morphology of MgO precursor.[41] From the FT-IR spectra, one can observe that the absorption strength at 796 cm^{-1} followed the order of nanosheets > nanodisks > flower-like MgO morphology. It is noted that the absorption band located at 470 cm^{-1} characteristic for the stretching vibration of Mg-O-Si bonds was found over three composite samples.[42-43] The characteristic peak of the Mg-O-Si species exhibited the greatest intensity at the expense of Si-O-Si bonds, indicative of the strengthened interaction between flower-like MgO and SiO_2, preferentially generating a Mg-O-Si linkage.[44]

The UV-visible diffuse reflectance spectra of three MgO-SiO_2 composites with different morphology are shown in Fig.2. Notably, the flower-like sample shows an intense absorption peak near 260 nm whereas the nanodisks and nanosheets materials

exhibit much weaker absorption bands. According to the previously reported literature, the absorption at 260 nm can be attributed to the Mg-O-Si bond. [17, 26] Therefore, the morphology-dependent UV absorption can be related to the interaction of MgO and SiO_2 in the composites. The intense absorption at 260 nm over flower-like sample may be explained by the large amount of Mg-O-Si chemical bond formation resulted from the strong interaction of MgO and SiO_2, demonstrating the readily formation of special properties of Mg-O-Si chemical bonds by using flower-like MgO precursor, which is in good agreement with the results of FT-IR characterizations.

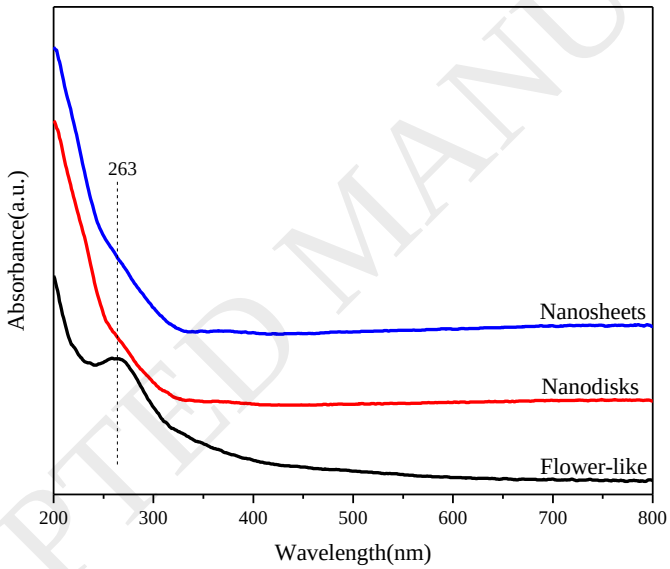

Fig.2. UV-vis diffuse-reflectance spectra of the catalysts with three different morphologies.

CO_2/NH_3 temperature-programmed desorption (CO_2/NH_3-TPD) were used to probe the surface acidic and basic properties of the catalysts to understand better their intrinsic acid/base functionalities, as shown in Fig. 3 and quantitative data were summarized in Table 2 and 3. In Fig. 3a and 3b, two broad desorption peaks of NH_3

and CO_2 were resolved near 150 °C and 250 °C for all catalysts, which were attributed to NH_3 and CO_2 chemisorbed on weak and medium acidic/basic sites, respectively. According to data presented in Table 2 and Table 3, flower-like catalyst possesses the most abundant basic sites, and nanosheets show the most acidic sites over the catalyst surface. The order of relative strength of surface base/acid sites is flower-like (0.97) > nanodisks (0.80) > nanosheets (0.63), suggesting the highly enhanced basicity by using flower-like MgO precursor.

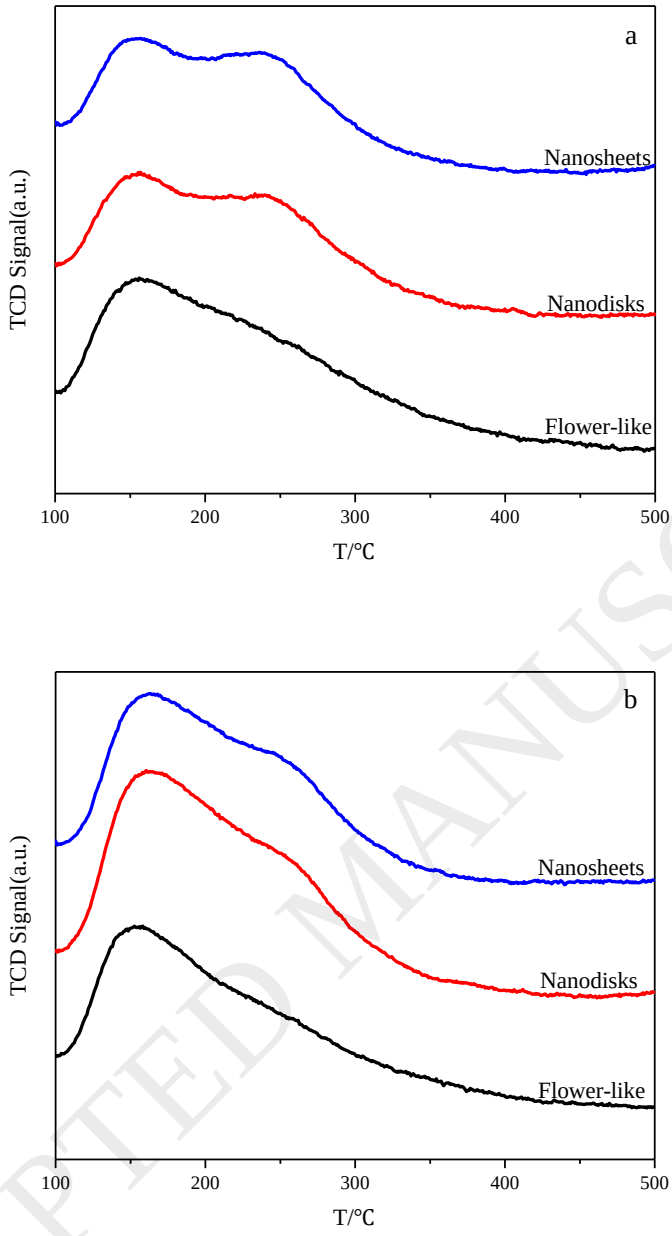

Fig.3. NH_3-TPD (a) profiles and CO_2-TPD (b) profiles for the MgO-SiO_2 catalysts with different morphologies.

Table 2 Summary of the amount of acidic sites over the different MgO-SiO_2 catalysts calculated via NH_3-TPD analysis.

Samples	Number of acidic sites(mmol/g)		
	Total sites (T_a)	Weak sites[a]	Moderate sites[b]
Flower-like	0.40	0.28	0.12

Nanodisks	0.45	0.30	0.15
Nanosheets	0.48	0.31	0.17

[a] The temperature range of weak acidic sites is 100~250 °C.

[b] The temperature range of moderate acidic sites is 250~500 °C.

Table 3 Summary of the amount of basic sites over the different MgO-SiO_2 catalysts calculated via CO_2-TPD analysis.

Samples	Number of basic sites(mmol/g)			
	Total sites (T_b)	Weak sites[a]	Moderate sites[b]	T_b/T_a
Flower-like	0.39	0.27	0.12	0.97
Nanodisks	0.36	0.26	0.10	0.80
Nanosheets	0.30	0.23	0.07	0.63

[a] The temperature range of weak basic sites is 100~250 °C.

[b] The temperature range of moderate basic sites is 250~500 °C.

In order to further understand the influence of morphology on the sruface acidity of the catalysts, pyridine adsorption was also examined by the FTIR to discriminate the surface Lewis acid sites and Brønsted acid sites. As shown in Fig. 4, the characteristic peaks of the acidic site adsorbed by pyridine appears in 1448 cm^{-1} for strong Lewis acid sites (SL), 1490 cm^{-1} for a combination of Lewis and Brønsted acid sites (B+L), 1537 cm^{-1} for Brønsted acid sites (B), 1577 cm^{-1} for weak Lewis acid sites (WL), 1607 cm^{-1} for strong Lewis acid sites (SL).[26] It can be seen from the infrared spectra that a strong absorption peaks can be observed at 1448 cm^{-1}, 1490 cm^{-1}, 1577 cm^{-1}, and 1607 cm^{-1}, indicating that all three materials contain Lewis acid sites. No characteristic absorption peak of Brønsted acid was observed at 1537 cm^{-1}, suggesting that Brønsted acid sites on related to SiO_2 have been considerably passivated by the strong interaction of SiO_2 with MgO and Lewis acid sites prevailed over the surface of all three samples. Moerover, the absorption peak intensity of Lewis acid sites

followed the order of flower-like < nanodisks < nanosheets, agreeing well the results of NH_3-TPD.

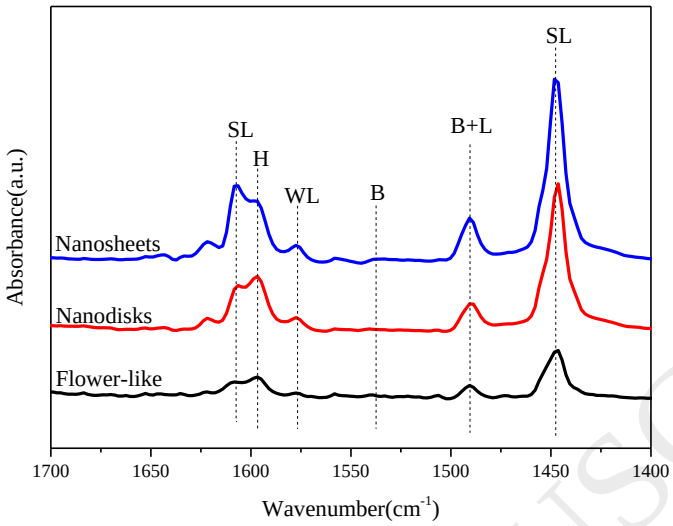

Fig.4. FTIR spectra for the MgO-SiO_2 catalysts with different morphologies after pyridine adsorption with the desorption temperature at 200 °C. The characteristic absorption peaks of pyridine on acidic sites are the following: Brønsted (B), weak Lewis (WL), strong Lewis (SL) and hydrogen bound pyridine (H).

3.2. Catalyst activity

Fig.5 displays the catalytic performance of the flower-like catalyst for ethanol to BD at WHSV of 4.1 h^{-1}. Acetaldehyde, 1,3-BD and ethylene were the only quantified carbon-containing products, and no other compounds such as carbon dioxide, acetic acid and ethyl acetate were quantified because their content were very low. As shown in Fig. 5, ethanol conversion over flower-like catalyst increased with increasing reaction temperature up to 500 ^oC. With the increasing temperature, the selectivity for the desired product of BD increased first and went through a maximum of 63% when the temperature reach 400 °C, and as the temperature further increased, the selectivity of BD started to decline. The continuous increase of ethylene selectivity at the

expense of the decreasing acetaldehyde selectivity implies that the formation of ethylene and acetaldehyde follows a different parallel competitive reaction pathway. The continuous decreased acetaldehyde and the peak selectivity of BD in the whole temperature range strongly suggest that acetaldehyde and BD are the primary and secondary products in the cascade reaction sequences, respectively. The activity of the catalysts with two other morphologies was presented in FigureS4.

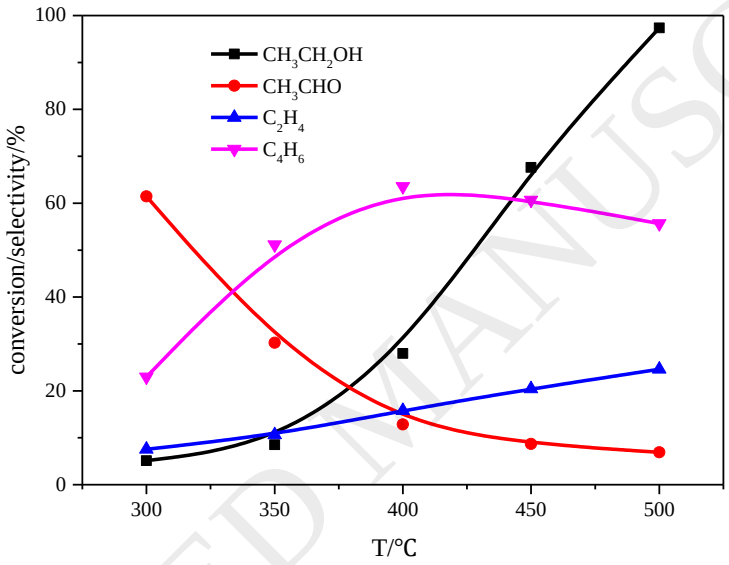

Fig.5. Temperature-dependent reactivity of the flower-like MgO−SiO_2 sample.(TOS: Product analysis taken by averaging two measurements within a TOS of 1.5 h at each temperature.)

The effect of the MgO precursor morphologies on the catalytic behavior of the MgO-SiO_2 catalysts were investigated for ethanol to BD at reaction temperature of 450 °C. It is evident in Fig. 6 that the activities of the samples in terms of ethanol conversion and BD selectivity decrease in the following order: flower-like >nanodisks>nanosheets. The superior activity of flower-like catalyst was correlated with the morphology-dependent strong metal oxide-support interaction, as estimated

by FT-IR, UV-Vis and chemisorption. Our activity data combined with the characterization results presented in this study illustrates that the morphology of MgO precursors is of prime importance on the interaction of MgO and SiO_2, and thus determines the catalytic activity in BD production. This conclusion is actually in consistent with the previous results which reported that the proper surface properties and the existence of Mg-O-Si bond are vital factor for catalytic efficiency.[30, 45]

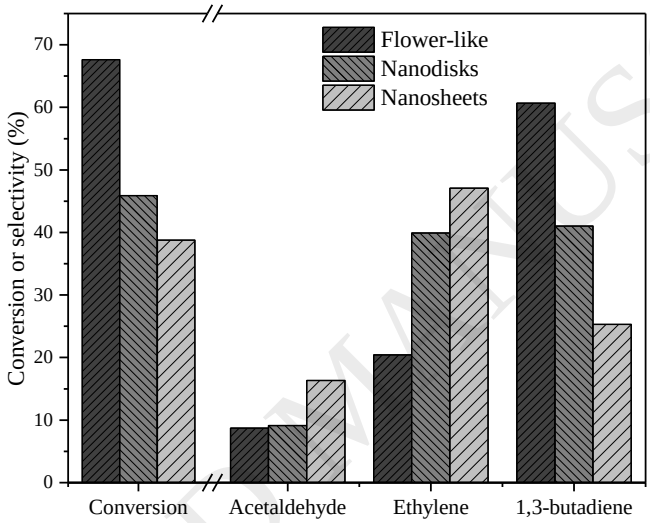

Fig.6. Comparison of catalytic behavior over three MgO−SiO_2 catalysts with different morphologies at 450 °C.

To further elucidate the nature of the conversion of ethanol to 1,3-BD, kinetic studies were performed to obtain the activation energy of the final product 1,3-BD. Fig. 7 shows the kinetic curves of three catalysts with different morphologies. From the data of the activation energy, it is easy to see that the activation energy of the flower-like catalyst showed the minimum energy of 157.4 KJ/mol, which indicate that the flower-like catalyst is the most active material to convert ethanol into 1,3-BD. By

comparing the specific surface area and activation energy data of the three catalysts, the flower-like catalyst has the smallest specific surface area and also the lowest activation energy, but has the highest activity, which excludes the factor that the catalyst activity is dominated by the specific surface area. These results indicate that the special structure formed by the catalyst itself and the proper acid-basic properties on the catalyst surface are the key factors affecting the catalytic activity.

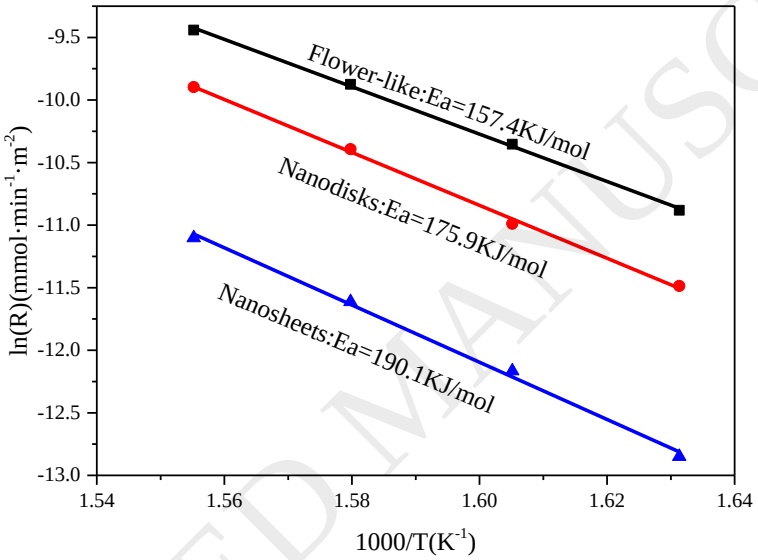

Fig.7. Arrhenius-type plots of 1,3-butadiene production rate over the catalyst with three different morphologies.

The stability of the flower-like catalyst was studied in Fig. S5. With the time on stream, the conversion rate of ethanol and the selectivity of butadiene decreased gradually, which may be due to the carbon deposition on the catalyst surface, resulting in the covering of active sites on the surface. After 40 hours of reaction, the conversion rate of ethanol decreased from 71.6% to 52.9% while the selectivity of 1,3-BD still maintained above 54.5%. The respective selectivity of the main

byproducts for ethylene and acetaldehyde did not increase significantly after 40 h of time on stream. From these data, the MgO-SiO_2 catalyst is relatively stable under the reaction conditions.

3.3. The implication of morphology effect on ethanol conversion to BD

It is well known that MgO-SiO_2 composite catalysts have been regarded as a superior candidate in catalyzing the conversion of ethanol to BD. Numerous factors are closely relevant to catalytic activity, such as BET surface areas, surface acid-base properties, the existence of active phase, and morphology. Based on the aforementioned catalytic data and characterization results, the morphology-dependent surface properties contribute a momentous portion to the highly enhanced performance of flower-like MgO-SiO_2 catalyst. The differences in surface acid-base properties of the catalysts were also confirmed by CO_2 and NH_3-TPD. A comparison of the ratio of surface acidic and basic sites obtained from CO_2/NH_3-TPD showed increased basicity over the flower-like sample. The enhanced surface basicity may facilitate the key reaction step of ethanol dehydrogenation and sequential aldol condensation, which occurs favorably over basic sites of the multifunctional catalysts.

To further understand the interaction of ethanol and catalyst surface, ethanol-TPD was used to investigate the dependence of the reaction pathways on the surface acid-base properties of the catalysts synthesized by different MgO morphologies. As shown in scheme 1,[46] dehydrogenation and dehydration occur competitively in parallel over the surface of the MgO-SiO_2 catalysts, depending on the nature of the surface acid-base properties. Figure 8 displays TPD data obtained following ethanol

pre-adsorption over catalyst surface. The main desorbed species were identified as CH_3CHO, H_2, C_4H_6 (1,3-BD), C_2H_4 and CH_3CH_2OH. Notably, three CH_3CHO and H_2 peaks are observed over these MgO-SiO_2 catalysts in Fig. 8a and Fig. 8b. The first CH_3CHO peak at low temperature below 200 ^oC was attributed to the dehydrogenation of adsorbed ethanol on catalyst surface, which was further confirmed by the presence of H_2 in the same temperature range. The absence of the second CH_3CHO peak in the intermediate temperature range over flower-like sample may be explained by the highly enhanced surface reaction of ethanol at the expense of CH_3CHO, as evidenced by the intense peak for C_4H_6 and H_2 in the same temperature range. The simultaneous desorption of CH_3CHO and H_2 at high temperatures is due to the inhibited aldol condensation of CH_3CHO molecules at temperatures above 400 ^oC. Based on the above analysis, combined with the desorption profiles of ethanol in Figure 8e, it was found that the peak intensity of ethanol desorption followed the order of flower-like < nanodisks < nanosheets, in reversed order of activity data. This result is consistent with the results of the catalytic activity in Section 3.2. Moreover, the ratio of basic sites/acid sites varies in the order: flower-like (0.97) > nanodisk (0.80) > nanosheet (0.63). This is in the same order of intensity ratio of CH_3CHO and C_4H_6 formed over these MgO-SiO_2 catalysts. In this work, the strong interaction between MgO and SiO_2 can passivate the strong Brønsted acidic sites of SiO_2 by forming a Mg-O-Si bond, and generate new Lewis acid-base site pairs with enhanced electron cloud density on the bridged O (i.e., 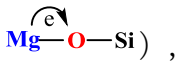

), which not only facilitates the dehydrogenation of ethanol to acetaldehyde, but also boosts the reactivity of

acetaldehyde to aldol condensation, thereby increasing the 1,3-butadiene productivity. C_2H_4 desorption peaks display higher intensity over nanosheet sample than over flower-like and nanodisk catalysts.Correlating the NH_3-TPD spectra and the data listed in Table 2, a relationship between the population of surface acidic sites and C_2H_4 generation can be well established, agreeing well with the literature reports.[20, 22, 47]

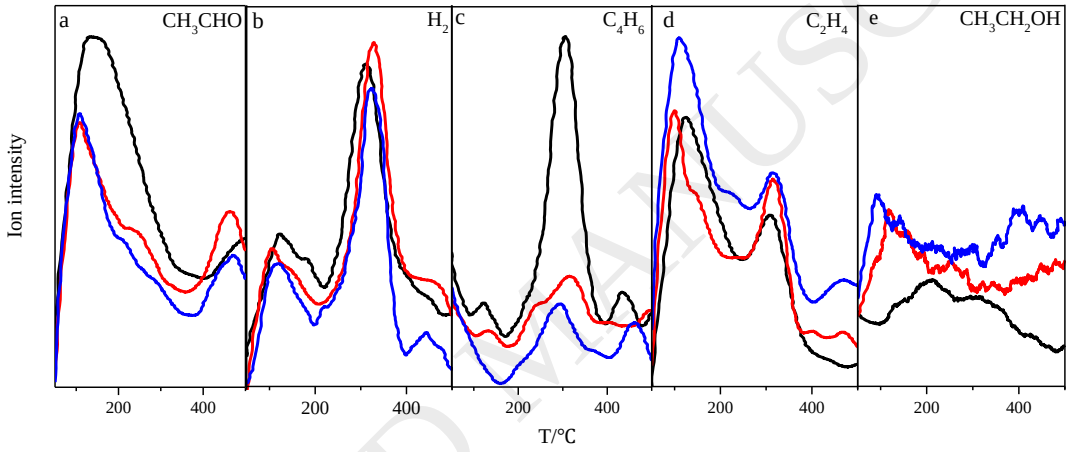

Fig.8. Desorption profiles of major products from ethanol-TPD over MgO-SiO_2 catalysts (Flower-like; Nanodisks; Nanosheets)

The ^{29}Si MAS NMR was used to investigate the changes in the chemical environment around Si and provided a basis for a better understanding of the impact of interfacial Mg-O-Si linkage on the catalytic efficiency. The ^{29}Si MAS NMR spectra of MgO-SiO_2 catalyst with different morphologies was presented in Fig. 9. It is known that the signal intensity in these ^{29}Si MAS NMR spectra depends on the density of ^{1}H around the ^{29}Si core and the distance of ^{1}H-^{29}Si in these species. The

shorter ^{1}H-^{29}Si distance usually leads to a greater density, and therefore results in a highly enhanced signal intensity of ^{29}Si.NMR spectra of the MgO-SiO_2 catalysts show chemical shift signals appearing around -110 ppm, -93 ppm, -90 ppm, -86 ppm, -83 ppm, and -76 ppm. As reported in the previously literature,[26, 45, 48] the signal at -110 ppm is attributed to a Si atom containing four siloxane bonds ($Si^*(OSi)_4$), and the signal at -93 ppm should be the intermediate phase ($Si^*(OH)(OSi)_3$) during formation, -90 ppm corresponds a Si atom having two siloxane bonds and two hydroxyl groups ($Si^*(OSi)_2(OH)_2$),-83 ppm is due to an enstatite phase intermediate, -86 ppm and -76 ppm are attributed to Mg-O-Si bond in the form of $Si^*(OMg)(OSi)_2(OH)$ and $Si^*(OMg)_2(OSi)_2$. It can be seen from NMR spectra of samples with three different morphologies that the spectra at nanodisks and nanosheets show the distinct signals located at -83 ppm and -110 ppm, and the very weak signals at -86 ppm and -76 ppm, indicating the weak interaction between MgO and SiO_2 during the course of the formation of the nanodisk and nanosheet composite catalysts. By contrast, the ^{29}Si MAS NMR spectra of the flower-like catalyst display distinct signals of chemical shift at -93 ppm, -90 ppm, -86 ppm, and -76 ppm. The strong signal at around -86 and -76 ppm suggest that the use of silica sol during the preparation of the catalyst resulted in the formation of an amorphous surface magnesium silicate phase[26, 45], and generated much more intense peaks corresponding to Mg-O-Si bonds in the form of $Si^*(OMg)(OSi)_2(OH)$ and $Si^*(OMg)_2(OSi)_2$. Meanwhile, the strong intensity at -90 ppm and -93.9 ppm also suggests that SiO_2 still partially retained its original phase during the preparation of the flower-like catalyst.

These results indicate that the use of MgO with different morphologies during the impregnation followed by the subsequent calcination leads to the formation of interfacial Mg-O-Si chemical bond. Similar results were observed previously by Sels and co-workers for Ag/MgO-SiO_2 catalysts prepared by impregnation.[26] Such behavior is not unexpected taking into account the recent work revealed that the surface acid-base change with the generation of new Lewis acid-base pairs with enhanced Lewis basicity on the bridged O in Zr-O-Zn pair, which in turn affect the reactivity in cascade conversion of ethanol to lower olefins. [49-50]

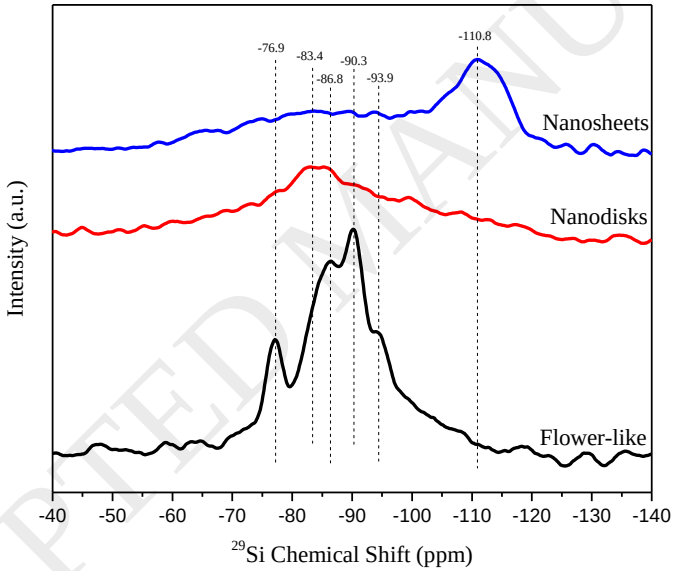

Fig.9. ^{29}Si MAS NMR patterns of the MgO−SiO_2 catalysts with different morphologies.

As documented in the literature, the key factors determining the activity and selectivity of mixed oxides prepared are assumed to be the morphology (surface area and pore size) and the relative proportions of M1-O-M to M-O-M bonds.[51] For instance, the catalytic activity of olefins epoxidation on TiO_2-SiO_2 mixed oxides has

been strongly correlated with the Ti-O-Si connectivity that is characteristic of Ti dispersion in the silica matrix.[52] The formation of Ti-O-Si bonds strongly modifies the electronic structure of the bridge oxygen and titanium atoms at the interface of TiO_2/SiO_2 multilayers. Wachs et al.[53-54] suggest that strong interactions between oxides tend to form bridge oxygen bonds, which in turn alter the electronic properties between the elements, increase the electron cloud density of the O atoms, resulting in an enhanced bacisity and therefore the boosted performance of methanol oxidation over the mixed oxide catalysts. The recent reports by Wang et al.[49] and us[50] also suggested that the strong interaction between ZnO and ZrO_2 favors the formation of Zn-O-Zr bond with enhanced Lewis-basicity of the bridged O, which further promotes the reactivity of the aldol condensation reaction involved in the formation of isobutene. Recently, Toshihide[55] et al. proposed that the electron cloud density of the O atom on the bridge oxygen bond may play a crucial role in the reaction of ethanol to 1,3-BD. The O atom in the structure of Mg-O-Ge was found to have the strongest electron cloud density and the lowest BE, as confirmed by XPS and DFT calculation. Therefore, the increase of electron density and the reductive character of the Mg-O-Ge structure can promote the crotonaldehyde formation from acetaldehyde and the reaction of crotonaldehyde reduction to crotyl alcohol due to an increase in basicity. In this work, results from FT-IR, UV-vis, and ^{29}Si MAS NMR data evidenced that the reinforced interaction between MgO and SiO_2 promotes the formation of new acid-base active structure by modulating the underlying MgO morphologies. The strong interaction between MgO and SiO_2 can passivate the strong

Brønsted acidic sites of SiO_2 by forming a Mg-O-Si bond, and generate new Lewis acid-base site pairs with enhanced electron cloud density on the bridged O (i.e., 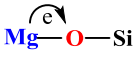) , which not only facilitates the dehydrogenation of ethanol to acetaldehyde, but also boosts the reactivity of acetaldehyde to aldol condensation, thereby increasing the 1,3-butadiene productivity. The activity data can be satisfactorily explained by the measurements based on FTIR, UV-vis, CO_2/NH_3/ethanol-TPD and ^{29}Si MAS NMR. Our investigations point to the direction of improving the intrinsic catalytic activity of MgO-SiO_2 catalysts via modulating the morphology of MgO-SiO_2 catalysts with more favorable flower-like morphology and porpulation of the Mg-O-Si linkages in this case, which is also in good agreement with the literature reports. Consequently, the surface properties of samples may be governed by the choice of MgO precursors, which then dictate the ethanol to 1,3-BD reactivity. The differences between the catalytic behaviors of samples prepared by MgO with different morphologies are well established based on the obtained results.

4. Conclusions

In this study, a series of catalysts with different morphologies were prepared using a reverse impregnation method (i.e. impregnating a silica sol onto MgO precursor). The effect of MgO precursor morphologies was explored for conversion of ethanol to 1,3-BD. In order to achieve high BD selectivity, the morphologies of MgO precursor is crucial and the use of flower-like MgO precursor was particularly successful in

promoting the high yield of BD while suppressing the formation of ethylene via ethanol dehydration. At the optimal reaction conditions, the best-performing flower-like catalyst exhibited ethanol conversion of 68% and BD selectivity of 61% at a high WHSV of 4.1 h^{-1} and 450 °C. Extensive characterizations demonstrate that the unique layered flower-like architectures may facilitate the formation of interfacial Mg-O-Si species and enhance Lewis basicity on the bridged O in Mg-O-Si bond via the strong interaction between MgO and SiO_2 in binary MgO-SiO_2 composite catalysts which are favorable for the superior activity. This work identifies the importance of morphological control of MgO-SiO_2 bifunctional catalysts on the effectiveness for cascade conversion of bio-ethanol to 1,3-butadiene.

Acknowledgements

This research was supported by the Program for Professor of Special Appointment (Eastern Scholar) at Shanghai Institutions of Higher Learning, the Talent Program of Shanghai University of Engineering Science, National Natural Science Foundation of China (21503133), Science and Technology Commission of Shanghai Municipality (18030501100), and Shanghai Talent Development Foundation (2017076).

References

[1] E. V. Makshina,W. Janssens,B. F. Sels ,P. A. Jacobs, *Catalysis Today*, **2012**, *198*, 338-344.

[2] E. V. Makshina,M. Dusselier,W. Janssens,J. Degreve,P. A. Jacobs ,B. F. Sels, *Chem Soc Rev*, **2014**, *43*, 7917-53.

[3] M. D. Jones, *Chemistry Central Journal*, **2014**, *8*, 53.

[4] C. Angelici,B. M. Weckhuysen ,P. C. Bruijnincx, *ChemSusChem*, **2013**, *6*, 1595-614.

[5] T. Yan,W. Dai,G. Wu,S. Lang,M. Hunger,N. Guan ,L. Li, *ACS Catalysis*, **2018**, *8*, 2760-2773.

[6] W. C. White, *Chemico-Biological Interactions*, **2007**, *166*, 10-14.

[7] P. C. Bruijnincx ,B. M. Weckhuysen, *Angew Chem Int Ed Engl*, **2013**, *52*, 11980-7.

[8] J. Goldemberg, *Science*, **2007**, *315*, 808-810.

[9] S. I. George W. Huber, and Avelino Corma, *Chemical Reviews*, **2006**, *106*, 4044-4098.

[10] P. Anbarasan,Z. C. Baer,S. Sreekumar,E. Gross,J. B. Binder,H. W. Blanch,D. S. Clark ,F. D. Toste, *Nature*, **2012**, *491*, 235-9.

[11] V. L. Sushkevich,Ivanova, II,V. V. Ordomsky ,E. Taarning, *ChemSusChem*, **2014**, *7*, 2527-36.

[12] V. L. Sushkevich,D. Palagin ,I. I. Ivanova, *ACS Catalysis*, **2015**, *5*, 4833-4836.

[13] S. Da Ros,M. D. Jones,D. Mattia,J. C. Pinto,M. Schwaab,F. B. Noronha,S. A. Kondrat,T. C. Clarke ,S. H. Taylor, *ChemCatChem*, **2016**, *8*, 2376-2386.

[14] T. De Baerdemaeker,M. Feyen,U. Müller,B. Yilmaz,F.-S. Xiao,W. Zhang,T. Yokoi,X. Bao,H. Gies ,D. E. De Vos, *ACS Catalysis*, **2015**, *5*, 3393-3397.

[15] J. V. Ochoa,C. Bandinelli,O. Vozniuk,A. Chieregato,A. Malmusi,C. Recchi ,F. Cavani, *Green Chemistry*, **2016**, *18*, 1653-1663.

[16] M. S. Niiyama Hiroo , Echigoya Etsuro ,, *Bulletin of the Chemical Society of Japan*, **1972**, *45*, 655-659.

[17] A. A. S. KVISLE, R.P.A. SNEEDEN, *Applied Catalysis*, **1988**, *43*, 117-131.

[18] M. D. Jones,C. G. Keir,C. D. Iulio,R. A. M. Robertson,C. V. Williams ,D. C. Apperley, *Catalysis Science & Technology*, **2011**, *1*, 267.

[19] C. Angelici,M. E. Velthoen,B. M. Weckhuysen ,P. C. Bruijnincx, *ChemSusChem*, **2014**, *7*, 2505-15.

[20] M. Lewandowski,G. S. Babu,M. Vezzoli,M. D. Jones,R. E. Owen,D. Mattia,P. Plucinski,E. Mikolajska,A. Ochenduszko ,D. C. Apperley, *Catalysis Communications*, **2014**, *49*, 25-28.

[21] Z. Han,X. Li,M. Zhang,Z. Liu ,M. Gao, *RSC Advances*, **2015**, *5*, 103982-103988.

[22] M. León,E. Díaz ,S. Ordóñez, *Catalysis Today*, **2011**, *164*, 436-442.

[23] M. León,E. Díaz,A. Vega,S. Ordóñez ,A. Auroux, *Applied Catalysis B: Environmental*, **2011**, *102*, 590-599.

[24] C. Angelici,M. E. Z. Velthoen,B. M. Weckhuysen ,P. C. A. Bruijnincx, *Catalysis Science & Technology*, **2015**, *5*, 2869-2879.
[25] M. Zhang,M. Gao,J. Chen ,Y. Yu, *RSC Advances*, **2015**, *5*, 25959-25966.
[26] W. Janssens,E. V. Makshina,P. Vanelderen,F. De Clippel,K. Houthoofd,S. Kerkhofs,J. A. Martens,P. A. Jacobs ,B. F. Sels, *ChemSusChem*, **2015**, *8*, 994-1008.
[27] Y. M. Rong He, Jixing Liu, Jinguo Wang, Wei An, Xiaoxiong Huang, Weiyu Song, Jian Liu, Sheng Dai, *ChemCatChem*, **2018**, *10*, 3969-3973.
[28] Y. M. Feng Liu, Jinguo Wang, Xiaoxiong Huang, Yuanqiang Wang Wei An, *ChemCatChem*, **2017**, *9*.
[29] L. Zhang,T. N. Pham,J. Faria,D. Santhanaraj,T. Sooknoi,Q. Tan,Z. Zhao ,D. E. Resasco, *ChemSusChem*, **2016**, *9*, 736-48.
[30] X. Huang,Y. Men,J. Wang,W. An ,Y. Wang, *Catalysis Science & Technology*, **2017**, *7*, 168-180.
[31] R. Palacio,J. Gallego,Z. Gabelica,C. Batiot-Dupeyrat,J. Barrault ,S. Valange, *Applied Catalysis A: General*, **2015**, *504*, 642-653.
[32] S. B. Simonsen,K. Agersted,K. V. Hansen,T. Jacobsen,J. B. Wagner,T. W. Hansen ,L. T. Kuhn, *Applied Catalysis A: General*, **2015**, *489*, 147-154.
[33] Z. Guo,C. Zhou,D. Shi,Y. Wang,X. Jia,J. Chang,A. Borgna,C. Wang ,Y. Yang, *Applied Catalysis A: General*, **2012**, *435-436*, 131-140.
[34] Z. M. Cui,Z. Chen,C. Y. Cao,W. G. Song ,L. Jiang, *Chem Commun (Camb)*, **2013**, *49*, 6093-6095.
[35] F. Wang,N. Ta ,W. Shen, *Applied Catalysis A: General*, **2014**, *475*, 76-81.
[36] Y.-h. Xie,B. Li,W.-Z. Weng,Y.-P. Zheng,K.-T. Zhu,N.-W. Zhang,C.-J. Huang ,H.-L. Wan, *Applied Catalysis A: General*, **2015**, *504*, 179-186.
[37] O. Isaienko ,E. Borguet, *Langmuir*, **2013**, *29*, 7885-95.
[38] P.-Y. Wu,Y.-P. Jiang,Q.-Y. Zhang,Y. Jia,D.-Y. Peng ,W. Xu, *New Journal of Chemistry*, **2016**, *40*, 2878-2885.
[39] A. J. M. B. A. Morrow, *The Journal of Physical Chemistr*, **1992**, *96*, 1395-1400.
[40] G. D. Basudeb Karmakar, Dibyendu Ganguli, *Journal of Non-Crystalline Solids*, **2000**, *272*, 119-126.
[41] F. Balas,M. Rodríguez-Delgado,C. Otero-Arean,F. Conde,E. Matesanz,L. Esquivias,J. Ramírez-Castellanos,J. Gonzalez-Calbet ,M. Vallet-Regí, *Solid State Sciences*, **2007**, *9*, 351-356.
[42] B. González-Rodríguez,R. Trujillano,V. Rives,M. A. Vicente,A. Gil ,S. A. Korili, *Applied Clay Science*, **2015**, *118*, 124-130.
[43] M. U. Ali Ġmran VAĠZOĞULLAR, Ġbrahim KULA, *International Journal of Environment*, **2015** *4*, 19-31.
[44] Y. Y. Li,K. K. Han,W. G. Lin,M. M. Wan,Y. Wang ,J. H. Zhu, *Journal of Materials Chemistry A*, **2013**, *1*, 12919.
[45] Q. Zhu,B. Wang ,T. Tan, *ACS Sustainable Chemistry & Engineering*, **2016**, *5*, 722-733.
[46] T. N. P. Lu Zhang, Jimmy Faria, Daniel E. Resasco, *Applied Catalysis A:*

General, **2014**, *504*, 119-129.

[47] S. L. Guangwen Chen , Fengjun Jiao, Quan Yuan, *Catalysis Today*, **2007**, *125*, 111-119.

[48] C. A. Sang-Ho Chung, Stijn O.M. Hinterding, Markus Weingarth, Marc Baldus, Klaartje Houben, Bert M. Weckhuysen, and Pieter C.A. Bruijnincx., *ACS Catalysis*, **2016**, *6*, 4034-4045.

[49] J. S. Rebecca A.L. Baylon, Libor Kovarik, Mark Engelhard, Houqian Li, ,Y. W. Austin D. Winkelman, *Applied Catalysis B: Environmental*, **2018**, *234*, 337–346.

[50] B. Zhao,Y. Men,A. Zhang,J. Wang,R. He,W. An ,S. Li, *Applied Catalysis A: General*, **2018**, *558*, 150-160.

[51] R. Hutter,T. Mallat, A. Baiker, *Journal of Catalysis*, **1995**, *153*, 177-189.

[52] R. Hutter,T. Mallat, A. Baiker, *Journal of Catalysis*, **1995**, *157*, 665-675.

[53] I. E. Wachs, Loyd J. Burcham, *Catalysis Today*, **1999**, *49*, 467-484.

[54] I. E. Wachs, Goutam Deo, *Journal of Catalysis*, **1994**, *146*, 323-334.

[55] S. Akiyama,A. Miyaji,Y. Hayashi,M. Hiza,Y. Sekiguchi,T.-r. Koyama,A. Shiga ,T. Baba, *Journal of Catalysis*, **2018**, *359*, 184-197.